

Estimation of phase derivatives using discrete chirp-Fourier transform based method

Sai Siva Gorthi and Pramod Rastogi*

*Applied Computing and Mechanics Laboratory, Ecole Polytechnique Fédérale de Lausanne,
1015 Lausanne, Switzerland.*

**Corresponding author: pramod.rastogi@epfl.ch*

Estimation of phase derivatives is an important task in many interferometric measurements in optical metrology. This Letter introduces a new method based on discrete chirp-Fourier transform for accurate and direct estimation of phase derivatives, even in the presence of noise. The method is introduced in the context of the analysis of reconstructed interference fields in digital holographic interferometry. We present simulation and experimental results demonstrating the utility of the proposed method. © 2009 Optical Society of America

OCIS codes: 120.2650, 090.1995, 090.2880

Estimation of phase derivatives from interference fringe patterns has an important utility in many engineering applications as it directly provides the information on the strain distribution. Recently, increasing attention has been paid to the development of analysis methods [1–4] for obtaining a direct estimation of the phase derivatives. This Letter introduces a discrete chirp-Fourier transform based analysis method for accurate and direct estimation of phase derivative distributions. As an application, the method is here introduced in the context of analyzing reconstructed interference fields in digital holographic interferometry (DHI) [5]. Its applicability to other types of commonly used interferometers is also discussed.

DHI has emerged as a powerful non-invasive measurement and testing tool with applications in diverse areas of science and engineering. In DHI, the key parameter of interest is the phase of the reconstructed interference field, as the information on the measurand is encoded in it. The reconstructed interference field is given by:

$$A(x, y) = b(x, y) \exp [j\Delta\phi(x, y)] + \eta(x, y) \quad (1)$$

where $b(x, y)$ represents the amplitude variations, $\Delta\phi(x, y)$ is the interference phase whose derivative is to be estimated, and $\eta(x, y)$ is the noise term. The proposed technique relies on modeling each row/column of the reconstructed interference field as a piecewise-polynomial phase signal embedded in additive complex white Gaussian noise (ACWGN).

Each row/column of the reconstructed interference field is thus divided into different segments:

$$A_{yi} = b_{yi} \exp(j\Delta\phi_{yi}) + \eta_{yi} \quad (2)$$

where y , i and η represent the index of the row, the index of the segment and the ACWGN with zero-mean and σ^2 variance, respectively; y and i take values from 1 to N and 1 to N_w , respectively. The data in each segment can be approximated with a second-order polynomial phase signal:

$$g(x) = b(x) \exp [j(a_0 + a_1x + a_2x^2)] + \eta(x) \quad (3)$$

The derivative of phase can then be calculated as:

$$\frac{\partial\phi}{\partial x} = a_1 + 2a_2x \quad (4)$$

Equations (1)-(4) suggest that the problem of phase derivative estimation from Eq. (1) boils down to the problem of estimating the parameters a_1 and a_2 in Eq. (3). We propose the use of discrete chirp-Fourier transform (DCFT) for estimating $\{a_1, a_2\}$.

DCFT of $g(x)$ is defined as [6, 7]:

$$G(k_1, k_2) = \sum_{x=0}^{N_s-1} g(x) \exp [-j(\alpha_{k_1}x + \beta_{k_2}x^2)] \quad (5)$$

$$G(k_1, k_2) = FFT\{g(x) \exp [-j\beta_{k_2}x^2]\} \quad (6)$$

$$\text{where } \begin{cases} \alpha_{k_1} = \frac{2\pi}{N_s}k_1 & 0 \leq k_1 \leq N_s - 1 \\ \beta_{k_2} = \frac{2\pi}{N_s^2}k_2 & -N_s + 1 \leq k_2 \leq N_s - 1, \end{cases}$$

k_1 and k_2 are integers whose limits are specified as above, $N_s = N/N_w$ represents the number of samples present in a segment and $FFT\{\cdot\}$ denotes the fast Fourier transform operation. Just as the location of a peak in the Fourier transform domain of a single-tone provides information on a signal's frequency, the location of a peak in the DCFT-domain of a chirp-signal provides, simultaneously, information on the constant frequency and the chirp rate. In other words, the magnitude of DCFT achieves maximum when the values of α_{k_1} and β_{k_2} match respectively with the actual coefficients a_1 and a_2 of the signal's phase. Making use of this property, Fig. 1 illustrates the application of DCFT in determining the phase derivative of a 1-D signal. Fig. 1a shows the plot of the real part of the signal $g(x)$ synthesized with the polynomial coefficients $\{a_0 = -0.4702, a_1 = 0.9791, a_2 = -0.0076\}$ and amplitude $b(x) = 1$ at SNR of 20 dB. Magnitude of DCFT for $g(x)$ is shown in Fig. 1b; a dominant peak is clearly visible. Corresponding values of α_{k_1} and β_{k_2} at which the peak is seen to appear are 0.9817 and -0.0077 respectively. Because of the limited resolution (i.e., the step size used while generating α_{k_1} and β_{k_2}), the estimates are coarse and need further refinement.

One option for obtaining accurate estimates is to increase the resolution while computing DCFT. This is understandably achieved at the cost of increased computational time. The other option and to which we adhere to is to use these coarse estimates obtained using DCFT as the initial guess for the Nelder-Mead simplex search optimization [8]. The fine search algorithm is built using the FMINSEARCH function in MATLAB, which performs multi-dimensional unconstrained nonlinear minimization by implementing the Nelder-Mead simplex search algorithm. Phase derivative of $g(x)$ estimated by this process at SNR of 0 dB is plotted in Fig. 1c. Error in phase derivative estimation is shown in Fig. 1d.

The reconstructed interference field is analyzed by calculating the phase derivative, using Eq. (4), within each window of the segmented signal. The estimates for the coefficients a_1, a_2 in each window are determined following the procedure outlined in the above paragraphs.

Though the error in the estimation of phase derivative remains quite small within each window, its tendency to change rapidly towards the edges of the windows causes the overall error (of the whole row) to increase (Fig. 2a). To reduce the error, we have used a scheme of two layers of windows to create fifty-percent overlapping. The reconstructed data from these two layers is considered in such a way that the error will be minimum (Fig. 2b). To further minimize the error at the boundaries of the windows, median filtering can be applied on the estimated phase derivative map.

If the measurement application also requires the estimation of the phase distribution, it can be obtained by integrating the phase derivative map. Phase estimated in this manner, however, requires an offset correction as the constant of integration is unknown. The offset can be calculated by employing the same estimation procedure along a representative column/row. Note that this way of estimating phase directly provides the unwrapped phase distribution.

Fig. 3a shows the simulated fringe pattern (corresponding to a simulated reconstructed interference field) with an *SNR* of 10 *dB*. Figs. 3b, 3c show respectively the estimated phase derivative map along *y*-axis obtained using the proposed DCFT method, and its *cosine* generated for the purpose of illustration. Phase distribution calculated using the numerical integration of the derivative map is shown in Fig. 3d. It needs an offset correction as the phase distribution of all columns starts from zero. Fig. 3e shows the resulting phase after offset correction. Error in phase estimation is shown in Fig. 3f.

Results shown in Fig. 3 are obtained using overlapping windowing concept and by dividing each column of the pattern into eight segments ($N_w = 8$). Table 1 shows the performance of the proposed method in estimating the phase derivative of the fringe distribution shown in Fig. 3a at different SNR levels for both simple windowing and overlapping windowing concepts. It is evident that the proposed method provides quite accurate results when applied with overlapping windowing concept.

Computation of DCFT using FFT implementation (Eq. (6)) makes it computationally a very efficient tool. On the other hand, it has the limitation of being able to approximate the phase locally by a second-order polynomial only. However, by increasing the number of windows (i.e., by segmenting the signal into more number of pieces) the proposed method should be able to approximate accurately, within each segment, the phase of the signal with a polynomial of second order.

Experimental results shown in Fig. 4 substantiate the effectiveness of the proposed method for the estimation of phase and its derivative in DHI. It is moreover interesting to note that the proposed method can also be applied to other interferometric techniques. In the absence of spatial carrier, phase shifting can be used to produce the data in the form represented in Eq. (1) [4]. For carrier added/inherent fringe patterns, filtering operation to normalize the pattern [9], followed by real to analytic signal conversion using Hilbert transform, enables to arrive at Eq. (1).

To conclude, an estimation procedure based on discrete chirp-Fourier transform is introduced in this Letter for the determination of phase derivative, and eventually by its integration, of phase. Simulation and experimental results confirm that the proposed method provides an accurate estimation of directly the phase derivative maps even in the presence of noise. Calculation of phase by integrating the estimated phase derivative is also found to be a feasible solution for obtaining directly the unwrapped phase distribution.

This work is funded by Swiss National Science Foundation under Grant 200020-121555.

References

1. C. A. Sciammarella and T. Kim, *Exp. Mech.* **45**, 393 (2005).
2. Q. Kemao, S. H. Soon, and A. Asundi, *Appl. Opt.* **42**, 6504 (2003).
3. C. J. Tay, C. Quan, W. Sun, and X. Y. He, *Opt. Commun.* **280**, 327 (2007).
4. K. Qian, S. H. Soon, and A. Asundi, *Opt. Lett.* **28**, 1657 (2003).
5. U. Schnars and W. P. O. Juptner, *Meas. Sci. Tech.* **13**, R85 (2002).
6. X. Xia, *IEEE Trans. Sig. Proc.* **48**, 3122 (2000).
7. X. Guo, H. Sun, S. Wang, and G. Liu, *IEEE Trans. Sig. Proc.* **50**, 3115 (2002).
8. J. C. Lagarias, J. A. Reeds, M. H. Wright, and P. E. Wright, *SIAM Journal on Optimization* **9**, 112 (1999).
9. J. A. Guerrero, J. L. Marroquin, M. Rivera, and J. A. Quiroga, *Opt. Lett.* **30**, 3018 (2005).

Table 1: Performance evaluation of DCFT method ($N_w = 8$) with respect to noise

SNR	RMSE values	
	Simple Windowing	Overlapping Windowing
30 dB	0.0027	0.0017
20 dB	0.0041	0.0028
10 dB	0.0109	0.0076

List of Figures

Fig. 1 (a) Plot of the real part of $g(x)$, (b) Magnitude of the DCFT of $g(x)$, (c) Estimated phase derivative of $g(x)$, at SNR of 0 dB, after optimization, (d) Error in phase derivative estimation.

Fig. 2 (a) Comparison of error plots when simple windowing and overlapping windowing concepts are used, (b) Fifty-percent overlapping windowing scheme.

Fig. 3 (a) Simulated fringe pattern at SNR of 10 dB (256×256), (b) Estimated phase derivative along y-axis using the proposed DCFT method, (c) cosine of the phase derivative along y-axis (for illustration), (d) Phase obtained by the numerical integration of the derivative map shown in b, (e) Phase map after offset correction, (f) Error in phase estimation.

Fig. 4 (a) Recorded fringe pattern corresponding to the central loading of a circularly clamped object in a DHI experiment, (b) Phase derivative map along y-axis, (c) cosine of the phase derivative along y-axis (for illustration), (d) Phase distribution obtained by numerical integration of the derivative map shown in b, (e) Phase map after offset correction.

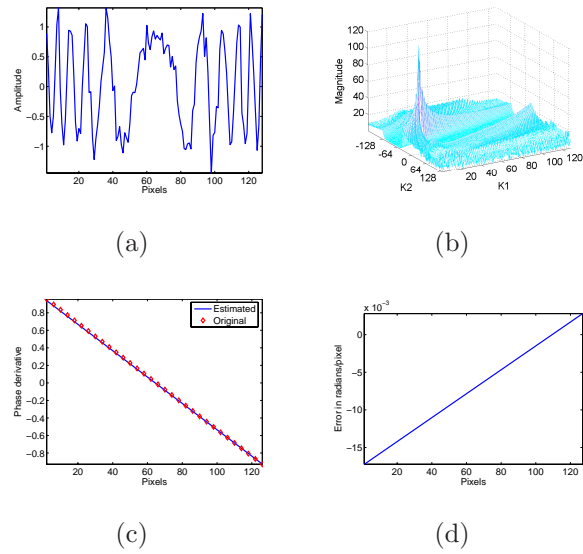


Fig. 1: (a) Plot of the real part of $g(x)$, (b) Magnitude of the DCFT of $g(x)$, (c) Estimated phase derivative of $g(x)$, at SNR of 0 dB, after optimization, (d) Error in phase derivative estimation.

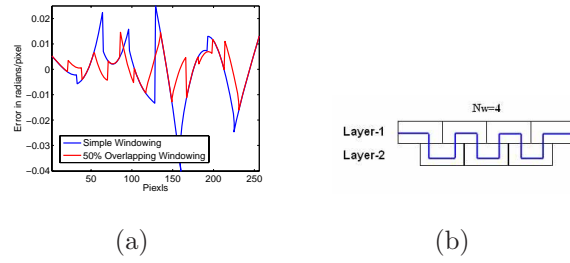


Fig. 2: (a) Comparison of error plots when simple windowing and overlapping windowing concepts are used, (b) Fifty-percent overlapping windowing scheme.

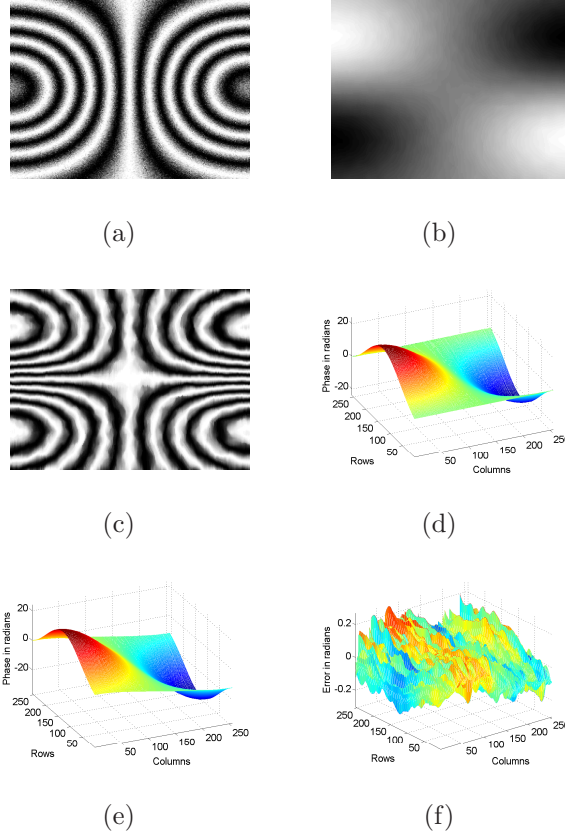


Fig. 3: (a) Simulated fringe pattern at SNR of 10 *dB* (256×256), (b) Estimated phase derivative along *y*-axis using the proposed DCFT method, (c) cosine of the phase derivative along *y*-axis (for illustration), (d) Phase obtained by the numerical integration of the derivative map shown in b, (e) Phase map after offset correction, (f) Error in phase estimation.

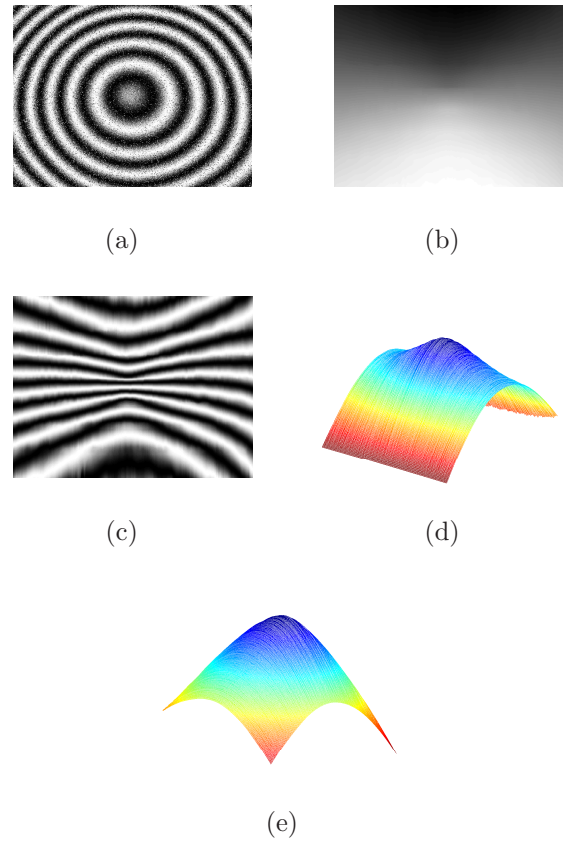


Fig. 4: (a) Recorded fringe pattern corresponding to the central loading of a circularly clamped object in a DHI experiment, (b) Phase derivative map along y-axis, (c) cosine of the phase derivative along y-axis (for illustration), (d) Phase distribution obtained by numerical integration of the derivative map shown in b, (e) Phase map after offset correction.